

Article

Assessment of Future Water Resources Availability under Climate Change Scenarios in the Mékrou Basin, Benin

Eric Adéchina Alamou ¹, Ezéchiél Obada ^{1,*} and Abel Afouda ^{1,2}

¹ Laboratory of Applied Hydrology, University of Abomey-Calavi (UAC), Cotonou 01 BP 4521, Benin; ericalamou@yahoo.fr (E.A.A.); aafouda@yahoo.fr (A.A.)

² West African Science Service Center on Climate Change and Adapted Land Use (WASCAL), GRP Climate Change and Water Resources, University of Abomey-Calavi (UAC), Abomey-Calavi BP 2008, Benin

* Correspondence: e.obada83@yahoo.fr; Tel.: +229-943-350-38

Received: 29 September 2017; Accepted: 8 November 2017; Published: 9 November 2017

Abstract: This work aims to evaluate future water availability in the Mékrou catchment under climate change scenarios. To reach this goal, data from Regional Climate Models (RCMs) were used as the input for four rainfall-runoff models which are ModHyPMA (Hydrological Model based on Least Action Principe), HBV (Hydrologiska Byråns Vattenbalansavdelning), AWBM (Australian Water Balance Model), and SimHyd (Simplified Hydrolog). Then the mean values of the hydro-meteorological data of three different projected periods (2011–2040, 2041–2070 and 2071–2100) were compared to their values in the baseline period. The results of calibration and validation of these models show that the meteorological data from RCMs give performances that are as good as performances obtained with the observed meteorological data in the baseline period. The comparison of the mean values of the hydro-meteorological data of the baseline period to their values for the different projected periods indicates that for PET there is a significantly increase until 2100 for both Representative Concentration Pathway 4.5 (RCP4.5) and RCP8.5 scenarios. Therefore, the rate's increase of potential evapotranspiration (PET) under the RCP8.5 scenario is higher than that obtained under the RCP4.5 scenario. Changes in rainfall amounts depend on the scenario of climate change and the projected periods. For the RCP4.5 scenario, there is a little increase in the annual rainfall amounts over the period from 2011 to 2040, while there is a decrease in the rainfall amounts over the other two projected periods. According to the RCP8.5 scenario, the contrary of changes observed with the RCP4.5 scenario are observed. At a monthly scale, the rainfall amounts will increase for August and September and decrease for July and October. These changes in rainfall amounts greatly affect yearly and monthly discharge at the catchment outlet. Over the three projected periods and for both RCP4.5 and RCP8.5, the mean annual discharge will significantly increase related to the baseline periods. However, the magnitude of increases will depend on the projected period and the RCP scenario. At a monthly scale, it was found that runoff increases significantly from August to November for all projected periods and the climate change scenario.

Keywords: climate change; rainfall-runoff models; water availability; student's test

1. Introduction

An international awareness of climate change and its consequences has been observed in recent decades. All communities, as a result of their daily experiences and IPCC (Intergovernmental Panel on Climate Change) reports [1], agree that extreme events will intensify. Climate change and variability issues have therefore become a focus of concern for scientists and policy makers around the world.

Projected temperatures and precipitation under different scenarios show that climate change will have different impacts on the various regions of the globe [2–5].

According to [5], Africa is one of the most vulnerable continents to climate change due to the diversity of effects and low adaptive capacity. Recent works on the West African region [6–8], under Representative Concentration Pathway (RCP4.5 and RCP8.5) scenarios of climate change projections, indicate that continued warming (1 °C to 6.5 °C) and a wider range of rainfall uncertainty (between –30% and 30%) will be observed in the Sahel until 2100. According to [9], the projected precipitation under RCP4.5 and RCP8.5 in the Mékrou catchment also indicates a wider range of precipitation uncertainties (roughly between –10% and 10%) and a decrease of about 10% in the number of wet days. The total intensity of precipitation for very wet days and the length of the dry spell period will increase until 2100 in the Mékrou catchment [9]. These changes could cause significant modifications to the hydrological regime of the catchment, especially at the end of the century and under the RCP8.5 scenario.

It is also reported by previous studies that the rainy seasons and the growing season will become shorter [10,11] in West Africa and the torrid, arid, and semi-arid climatic conditions will extend into the Sahel [6,12]. These climate changes will largely change the current balance of the water cycle. It is then necessary to predict the impacts of the changes on water resources. This requires hydrological modeling, which is a key step in any study of the impact of climate change on surface waters.

In the last decades, many studies on the future variability of rainfall [13–15] were carried out in West Africa. However, very few studies have evaluated the impacts of rainfall variability on future water resources. Moreover, the impacts of climate change on water resources have not been explored at short, medium, and long-term scales in the study area. This paper aims to analyze the recent and future variability of water resources in the Mékrou catchment.

2. Data and Methods

2.1. Study Area

The study area is the Mékrou catchment at the Kompongou outlet. Covering an area of 5670 km², it is located in the North of Benin between 1°30' and 2°15' East Longitude and 10°20' and 11°30' North Latitude (Figure 1). With an elongated shape, it covers three main cities (Kérou, Kouandé, and Péhunco). This catchment area belongs to the Benin side of the Niger basin. The highest point of the watershed is at Kampuya (639 m) around Kouandé, while the lowest point (266 m) is located around Kérou and precisely on the bed of the Mékrou River. The average slope of the stream bed is approximately 2.47%. The soil and the vegetation types in the basin are ferruginous soils on crystalline bedrock, histosols, swamps, and fertile gallery forests [16,17]. The rainfall amounts between 1981 and 2014 show that the months of July, August, and September are the wettest (Figure 2a). The discharge of the Mékrou River at Kompongou varies from 0 m³·s^{−1} in December to April to 100 m³·s^{−1} in September (Figure 2b). The annual mean of flow is about 21 m³·s^{−1}. High flows occur mostly during August to October.

2.2. Data

The data used in this study are of two types: observed data and simulated data from Regional Climate Models (RCMs) at a daily time step. The first are the observed rainfall, runoff, and potential evapotranspiration (PET) data. The rainfall and PET data were obtained from the Agency of Meteorology of Benin and the runoff data were obtained from the General Directorate of Water of Benin. Across the whole watershed, two rain gauges are available: Kouandé and Kérou. In addition to these two gauges, 12 rain gauges distributed around the basin are also available (Figure 1), resulting in a total of 14 rainfall stations. Over the period 1965–2010, all precipitation stations were functional. The PET data from the Natitingou synoptic station were considered as PET data in the basin.

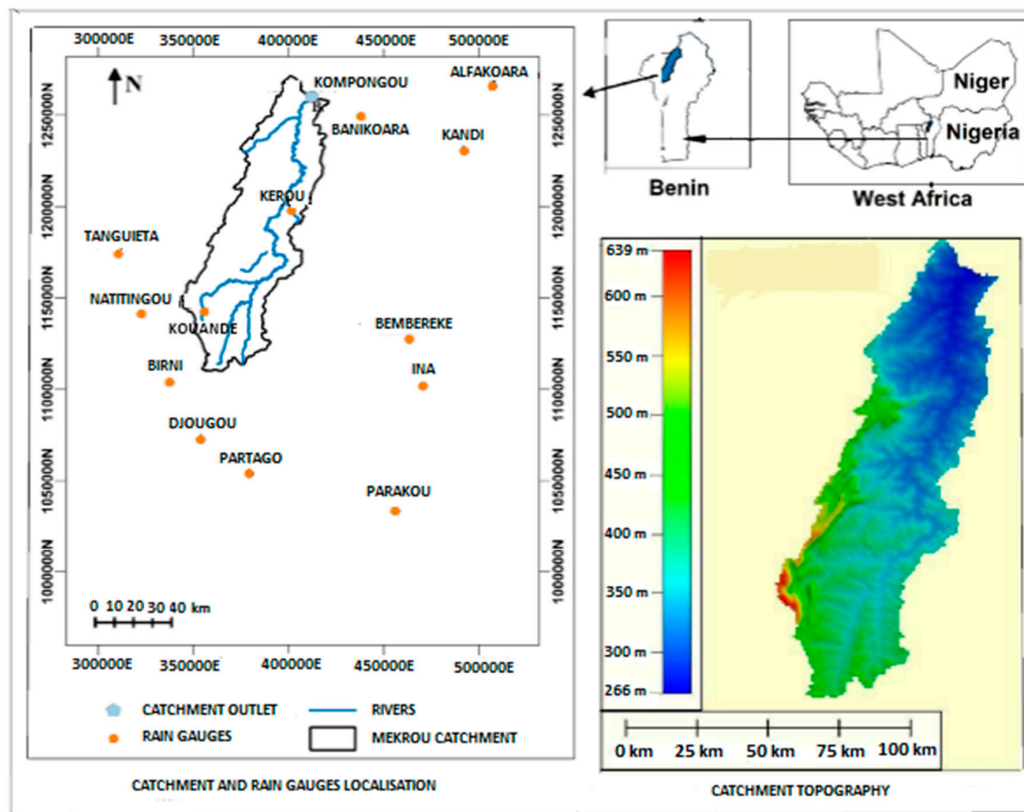


Figure 1. Study area.

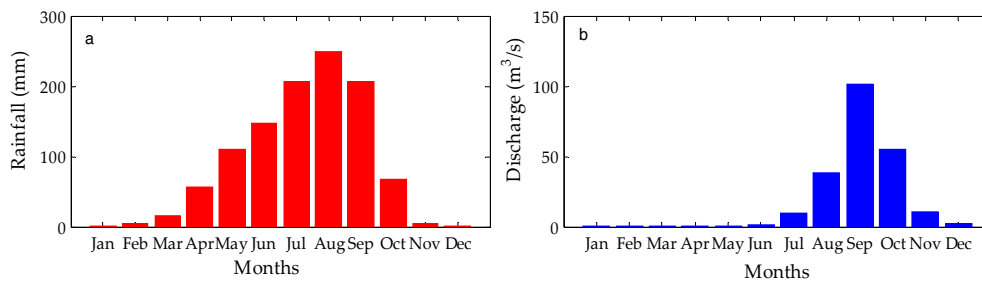


Figure 2. Seasonal variability of rainfall and discharge in the basin ((a) Monthly rainfall amounts over 1981–2014; (b) Monthly mean of discharge over 2006–2012).

The second are the simulated data. They are the historical and future projections (RCP4.5 and RCP8.5 scenarios) of rainfall and PET. These data are the three regional models’ (SMHI-RCA4 (Swedish Meteorological and Hydrological Institute-Rosby Centre Atmosphere model version 4), MPI-REMO (Max Planck Institute-Regional Model), DMI (Danish Meteorological Institute)-HIRHAM5) grid points located nearest to the ground-based weather stations obtained from the CORDEX (Coordinated Regional climate Downscaling Experiment) Africa project. The simulated rainfall were directly extract from the CORDEX Africa database, while the simulated PET were computed from the daily maximum temperature (T_{max} , °C), daily minimum temperature (T_{min} , °C), daily maximum humidity (RHmax, %), daily minimum humidity (RHmin, %), daily wind speed (WS, $m \cdot s^{-1}$) at a 2 m height, and daily sunshine duration (SD, h), also obtained from the CORDEX Africa project. These models are chosen because many studies (Akinsola, yacouba, Alioune, etc.) [13–15] in the West African region have recognized their ability to reproduce the rainfall regime. Their characteristics are shown in Table 1. The future projections were considered over the period from 2011 to 2100.

Table 1. Main characteristics of the RCM projections.

Model (RCM)	Institution	Driving GCM	Horizontal Resolution	No. of Vertical Levels	Simulation Period	Reference
HIRHAM5	DMI	GFDL-ESM2M	50 km	31	1951–2100	[18]
REMO	CSC	MPI-ESM-LR	50 km	27	1951–2100	[19]
RCA4	SMHI	EC-EARTH	50 km	40	1951–2100	[20]

2.3. Methodology

2.3.1. Bias Corrected Method

According to [1], in West Africa, climate models do not converge for the prediction of precipitation. For this, it is better to use a set of climate models in order to reduce the uncertainties of predictions. The precipitation and PET data from the three RCMs are used as an ensemble that represents the average of the three models. The RCM data were first averaged to create the ensemble, then the biases were corrected and finally the results were used as input data for the hydrological models. Ref. [21] corrected the bias of the precipitation simulated by each of these models and their ensemble with several bias correction methods and concluded that the Empirical Quantile Mapping (EQM) method (Equation (1)) [22] is the best of the used methods in this area. This method is used to correct the bias of RCM rainfall data. The EQM method is constructed by calculating the Probability Distribution Functions (PDF), while it uses the cumulative distribution functions (CDF) for the correction:

$$X_{cor} = F_{obs}^{-1}(F_{RCM}(X)) \quad (1)$$

where X_{cor} is the corrected meteorological parameter and X is the value simulated by the model; F_{RCM} is the CDF of the simulated data and F_{obs}^{-1} is the inverse of the CDF of the observed data.

2.3.2. Rainfall Interpolation Method

From the punctual daily rainfall series, the catchment average daily rainfall was calculated using the Kriging method [23–25]. The first step is to build the spatial structure of rainfall using a semivariogram, simply called a variogram. At the daily scale, the spherical model $\gamma_{mod}(h)$, shown by Equation (2), was adopted to fit the sample semivariogram. The interpolation was done by using the fitted semivariogram. A regular grid point was adopted, and an ordinary Kriging, which assumes an unknown mean as well as second-order stationary process, was implemented. At the end, the spatial rainfall mean for the study area was calculated as the statistical mean of the grid point values estimated by the ordinary Kriging for each day.

$$\gamma_{mod}(h) = S \left[3h/2a - 0.5(h/a)^3 \right] \quad (2)$$

where h is the distance between two rain gauges, S is the sill, and a is the range of the semivariogram.

2.3.3. Potential Evapotranspiration (PET) Estimation Method

Daily PET values are estimated using the Penman-Monteith method [26] expressed as:

$$PET = \frac{0.408\Delta(R_n - G) + \gamma \frac{900}{T + 273} u_2 (e_s - e_a)}{\Delta + \gamma(1 + 0.34u_2)} \quad (3)$$

where PET is the potential evapotranspiration ($\text{mm}\cdot\text{day}^{-1}$), R_n is the net radiation at the crop surface ($\text{MJ}\cdot\text{m}^{-2}/\text{day}$), G is the soil heat flux density ($\text{MJ}\cdot\text{m}^{-2}/\text{day}$), T is the mean daily air temperature at a 2 m height ($^{\circ}\text{C}$), u_2 is the wind speed at a 2 m height ($\text{m}\cdot\text{s}^{-1}$), e_s is the saturation vapour pressure

(kPa), e_a is the actual vapour pressure (kPa), $e_s - e_a$ is the saturation vapour pressure deficit (kPa), Δ is the slope vapour pressure curve ($\text{kPa} \cdot ^\circ\text{C}^{-1}$), and γ is the psychrometric constant (0.066) ($\text{kPa} \cdot ^\circ\text{C}^{-1}$).

2.3.4. Hydrological Models

To assess the future availability of water resources in the Mékrou basin, four hydrological lumped models were used. The use of different models can provide an average value of extrapolation or prediction that will be helpful in decision making. We chose lumped models because their parameterization is simple and their computation is efficient. Moreover, lumped models are better for long-term forecasts than distributed models. Indeed, lumped models do not explicitly take into account land use as distributed models. This is an asset because the prediction of long-term land use is unrealistic. The hydrological models used are: ModHyPMA (Hydrological Model based on Least Action Principe [27]), HBV (Hydrologiska Byråns Vattenbalansavdelning, Bergström and Forsman [28]), AWBM (Australian Water Balance Model, [29,30]), and SimHyd [31].

❖ ModHyPMA

ModHyPMA is a physics-based model (Figure 3a) with only two parameters to calibrate. The application of the Principle of Least Action results in the following differential equation [27,32]:

$$\frac{dQ}{dt} + \frac{\nu}{\lambda} Q^{2\nu-1} = \frac{X(t)}{\lambda} q(t) \quad (4)$$

where Q (mm/day) represents the discharge, t (day) represents the time, q (mm/day) represents the net rainfall, ν and λ are the model parameters, and X (mm) describes the state (dry or wet) of the catchment [32,33]. While ν expresses the nonlinearity of the physical phenomenon of water flow, λ is a macroscopic parameter that describes the properties related to the geomorphology and pedology of the catchment. When $\nu = 1$, λ has the dimension of time (d). For the nonlinear case (i.e., ν different from 1), the dimension of λ depends on the value of ν . By definition, ν and λ are physical parameters (they describe the physical structure of the system) and X is a process variable. The numerical solution of the differential equation gives an expression for the discharge:

$$Q_t = Q_{t-1} - \frac{\nu}{\lambda} Q_{t-1}^{2\nu-1} + \frac{X_t}{\lambda} q_{t-1} \quad (5)$$

where Q_t is the discharge at the outlet at time t ; Q_{t-1} is the discharge at the outlet at time $t - 1$; X_t describes the state of the catchment at time t ; and q_{t-1} is the net rainfall at time $t - 1$ ($X_t = \text{precipitation (P)} - \text{potential evapotranspiration (PE)}$, if $P > \text{PE}$).

For computation of the state of the soil, three new important assumptions were made:

- From day $t - 1$ to day t , the state X of the soil changes and X_t depends on X_{t-1} .
- The state of the soil is modified by the occurrence of precipitation: X_t is a function of X_{t-1} and q_t .

$$\text{if } P \geq \text{PE}, q_t = P - \text{PE}, \text{ otherwise } q_t = 0 \quad (6)$$

$$\begin{aligned} \text{if } q_t = 0, X_t &= X_{t-1} - \frac{\nu}{\lambda} X_{t-1} \\ \text{if } q_t \neq 0, X_t &= X_{t-1} + \frac{\nu}{\lambda} q_t^{2\nu-1} \end{aligned} \quad (7)$$

Equations (5)–(7) give, respectively, the formulas for the discharge, net rainfall, and state of the wetness of the catchment.

- The state of the soil X_t does not contribute to the discharge of day t as long as it is smaller than a threshold value TX .

In other words:

$$\text{if } X_t < TX, Q_t = Q_{t-1} - \frac{\nu}{\lambda} Q_{t-1}^{2\nu-1} \quad (8)$$

where TX is a parameter that is added to the model structure. In fact, in semi-arid and sub-humid areas, a certain amount of rainfall is required before discharge starts. In order to account for this amount, parameter TX has been introduced as a threshold [33]. The amount depends on catchment properties such as geology, topography, and land use. The value of TX is obtained by calibration. ModHyPMA is quite new and has been used for several Benin basins with better results than those of ‘Génie Rural à 4 paramètres Journaliers’ (GR4J) and HBV [32–34]. Ref. [35] compared the performance of nine lumped models and concluded that ModHyPMA is the most appropriate model for the application of this model in the Mékrou catchment.

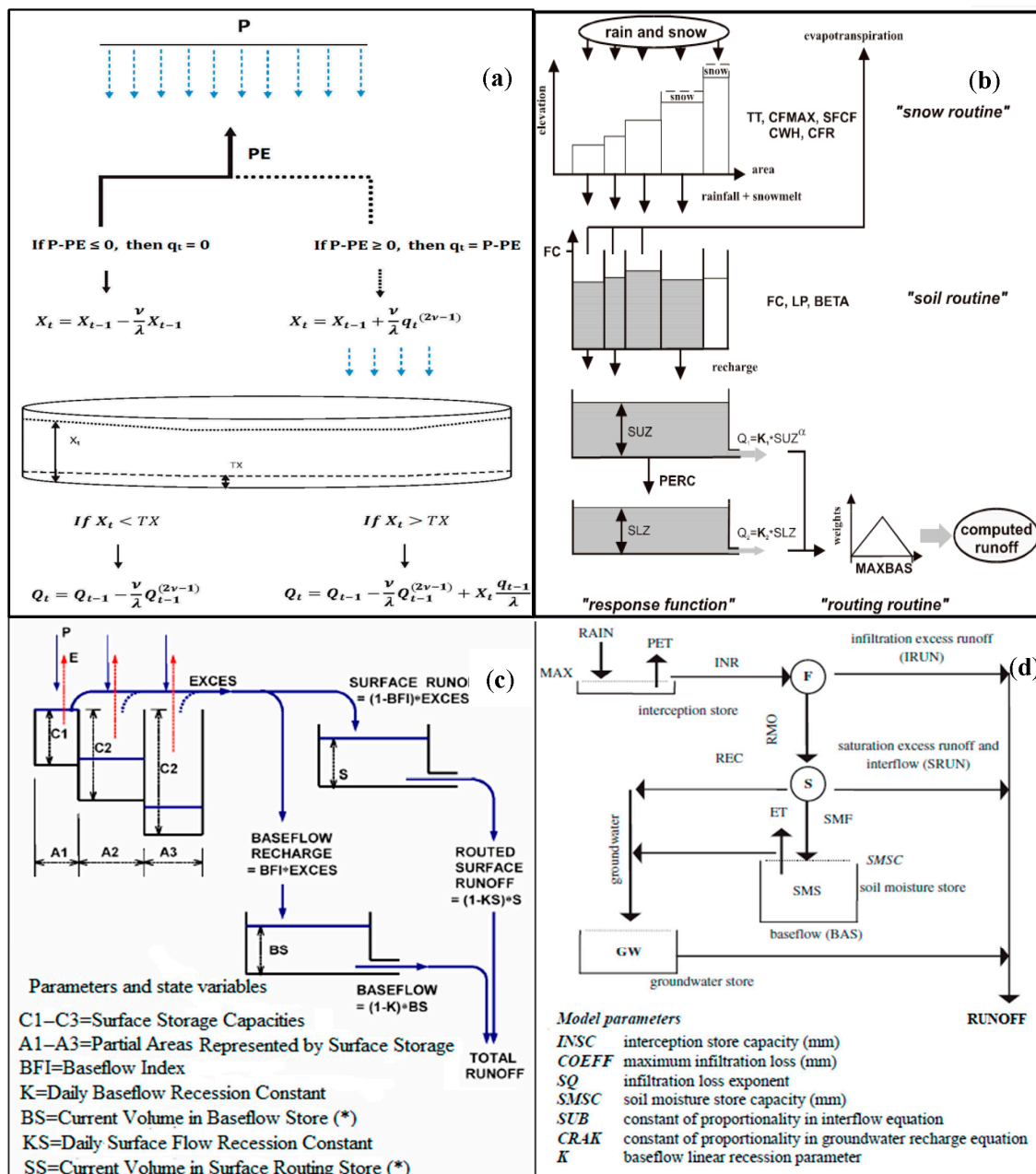


Figure 3. Schematic structure of (a) ModHyPMA [33]; (b) HBV [36]; (c) AWBM [37]; and (d) SimHyd [37].

❖ HBV

The light version of the HBV model, HBV-light [36], was also used to simulate runoff in this study. HBV-light is a conceptual lumped rainfall-runoff model that simulates catchment runoff at a daily time step and requires daily values of precipitation, air temperature, and potential evapotranspiration (based on either long-term daily or monthly averages) as input data. HBV-light has 14 parameters and it works with four routines (a snow routine, a soil moisture routine, groundwater routine, and a routing routine) [36]. Only the soil, groundwater, and routing routines were used in this study. The snow module was not activated this reduces the calibrate parameters to nine. The structure of HBV-light is shown in Figure 3b.

❖ AWBM

The Australian Water Balance Model (AWBM) is a conceptual lumped rainfall-runoff that calculates runoff from rainfall at daily or hourly time increments [30]. AWBM considers the catchment as having three surface stores (A1, A2, A3), each with its own storage capacities (C1, C2, C3). Each surface store is treated separately. The number of surface stores chosen is a pragmatic choice to reflect sufficient skill to simulate runoff without adding too many parameters and facing the risk of over-optimization [30]. At each time step, rainfall is added to each of the surface stores and evapotranspiration is subtracted. A portion of the rainfall excess (baseflow index time's rainfall excess) flows to the groundwater store, and the remainder becomes surface runoff. Baseflow from the groundwater store is simulated as a linear recession from the store. The total runoff is the sum of surface runoff and baseflow [30]. AWBM has seven parameters, as shown in Figure 3c.

❖ SimHyd

SimHyd is a daily lumped conceptual rainfall-runoff model that estimates daily stream flow. SimHyd simulates daily runoff (surface runoff and baseflow) using daily precipitation and PET as input data. The model estimates runoff generation from three sources: infiltration excess runoff, interflow (and saturation excess runoff), and base flow [31]. SimHyd has seven parameters and works with two storage reservoirs. The structure of the model is shown in Figure 3d.

2.3.5. Calibration Procedure

For the simulations of the four models, the same input data were used. The calibrated and validated periods are without missing discharge data. The simulation was acceptable if Nash-Sutcliffe Efficiency (NSE) > 0.5 and if we obtained a fairly good graphical fit. The calibrations of HBV-light, AWBM, and SimHyd were done by a genetic algorithm (optimization function) included in the HBV-light model [38] and in the RRL (Rainfall-Runoff Library), a software product in the Catchment Modelling Toolkit (eWater) [37]. The calibration of ModHyPMA was performed using stratified sampling of the parameter space as done by [33]. Assuming a uniform distribution of the model parameters, the parameter space of the parameters was divided into equidistant intervals. The model was run for all combinations of the model parameters searching for the global maximum in model performance. When required, the procedure was repeated with adapted parameter ranges. For all models, NSE (Equation (9)) was selected as the objective function. In addition to this criteria, the coefficient of determination (Equation (10)) was also used to compare the performances of the models. The models were calibrated over 10 years (1965–1974) and validated over five years (2007–2011).

$$\text{NSE} = 1 - \frac{\sum_{i=1}^n (Q_{i,obs} - Q_{i,calc})^2}{\sum_{i=1}^n (Q_{i,obs} - \bar{Q}_{obs})^2} \quad (9)$$

where $Q_{i,obs}$ is the daily observed discharge and $Q_{i,calc}$ is the daily simulated discharge. n represents the length of series and \bar{Q}_{obs} is the mean of observed discharge.

An NSE value of 0.5 for a comparison of the daily discharge is considered an acceptable value in some hydrological studies [39–41].

$$R^2 = \left[\frac{\sum_{i=1}^n (Q_{i,obs} - \bar{Q}_{obs})(Q_{i,calc} - \bar{Q}_{calc})}{\sum_{i=1}^n [(Q_{i,obs} - \bar{Q}_{obs})^2]^{0.5} \sum_{i=1}^n [(Q_{i,calc} - \bar{Q}_{calc})^2]^{0.5}} \right]^2 \quad (10)$$

where $Q_{i,obs}$ is the daily observed discharge and $Q_{i,calc}$ is the daily simulated discharge. n represents the length of series, \bar{Q}_{obs} is the mean of observed discharge, and \bar{Q}_{calc} is the mean of simulated discharge.

The value of R^2 describes the proportion of the variance of the observed flows with respect to the simulation flows. Authors such as [41] suggest that any R^2 value greater than 0.5 for daily flow comparisons is an acceptable threshold in hydrological simulations.

2.3.6. Change Rates

The rates of change were calculated by considering four different periods. The first period is the baseline period (1981–2010). The three other periods are the projected periods (2011–2040 (P1), 2041–2070 (P2), and 2071–2100 (P3)). For each hydro-meteorological variable and for each period, the mean and the standard deviation were calculated and then the rate of change was calculated as:

$$\text{Change rate} = \frac{\bar{X}_p - \bar{X}_r}{\bar{X}_r} \times 100 \quad (11)$$

where \bar{X}_p is the mean of a parameter over the considered projected period, and \bar{X}_r is the mean of the same parameter over the reference period.

2.3.7. Student's t -Test

To assess whether the means of the projected periods are statistically different from the mean of the baseline period, the student's t -test was used. Under the null-hypothesis of equal sample means ($H_0 : \bar{x}_1 = \bar{x}_2$) and alternate hypothesis of unequal sample means ($H_1 : \bar{x}_1 \neq \bar{x}_2$), the t -statistic is calculated as:

$$t = \frac{(\bar{x}_2 - \bar{x}_1)}{\sqrt{S_1^2/n_1 + S_2^2/n_2}} \quad (12)$$

where \bar{x}_1 and \bar{x}_2 are, respectively, the means of baseline and projected periods; S_1^2 and S_2^2 are, respectively, the variance of baseline and projected periods; and n_1 and n_2 are, respectively, the sizes of baseline and projected periods.

If $|t| < 1.96$, the difference between \bar{x}_1 and \bar{x}_2 is not statistically significant at the 95% confidence level.

If $|t| \geq 1.96$, the difference between \bar{x}_1 and \bar{x}_2 is statistically significant at the 95% confidence level.

3. Results

3.1. Change in Rainfall

3.1.1. Annual Change

Table 2 presents the means of annual rainfall amounts of the baseline period and the mean values of the three RCMs over the three different projected periods according to the RCP4.5 and RCP8.5 scenarios. It should be noted that for the baseline period (1981–2010), the mean of the annual rainfall amounts is 1048.86 mm with a standard deviation of 145.70 mm. Over the period from 2011 to

2040, the RCP4.5 scenario forecasts a slight increase in rainfall amounts compared to the reference period. This increase would be about 1% of the rainfall of the reference period. On the other hand, the RCP8.5 scenario predicts a reduction of about 5.30% of precipitation compared to the precipitation of the reference period. For the periods from 2041 to 2070 and from 2071 to 2100, the RCP4.5 scenario provides decreases of annual precipitation compared to the baseline period. These decreases are estimated to be about 6.30% of the baseline rainfall for the period from 2041 to 2070 against 1% for the period from 2071 to 2100. The RCP8.5 scenario provides an increase of rainfall over the period from 2041 to 2070 compared to the reference period, while a decrease of rainfall is indicated from 2071 to 2100. The rainfall surplus related to the baseline period is estimated to be about 2% over the period from 2041 to 2070 and a deficit of 1% is indicated for the period from 2071 to 2100. The decreases and increases of future rainfall amounts are not statistically significant at the 95% confidence level (Table 3). These results are consistent with those of [6], who predicted rates of change of −10% to 10% for future rainfall in West Africa and those of [10], who stated that precipitation projections are uncertain in the West.

Table 2. Mean and Standard deviation of rainfall over baseline and projected periods.

Baseline	Projections		
	Periods	RCP4.5	RCP8.5
1048.86 ± 145.70	P1	1054.79 ± 133.28	993.63 ± 134.48
	P2	982.86 ± 131.42	1067.14 ± 150.19
	P3	1035.38 ± 143.44	1038.28 ± 110.65

Table 3. Results of student’s t-test for rainfall amounts.

Periods	May	June	July	August	September	October	Yearly
RCP4.5							
P1	0.55	−3.72 *	−0.33	4.14 *	2.62 *	−2.40 *	0.16
P2	0.07	−4.95 *	−3.12 *	3.38 *	1.90	−2.41 *	−1.84
P3	−0.60	−7.12 *	−1.45	5.71 *	4.05 *	−2.74 *	−0.36
RCP8.5							
P1	0.78	−4.23 *	−3.31 *	3.45 *	2.81 *	−3.28 *	−1.53
P2	0.42	−2.17 *	−1.50	5.01 *	3.82 *	−1.54	0.48
P3	0.03	−4.83 *	−2.24 *	4.54 *	4.41 *	−3.14 *	−0.32

* States significant difference between the mean of the projected period and the mean the baseline period.

3.1.2. Monthly Change

Figure 4 shows the future change rates of monthly rainfall amounts for different projected periods under the RCP4.5 and RCP8.5 scenarios of climate change. According to these scenarios, the months of June, July, and October would exhibit deficit in rainfall amounts compared to the baseline period and with a pronounced decrease for the months of June and October. For the RCP4.5 scenario, the period from 2041 to 2070 exhibits the most deficit compared to the periods from 2011 to 2040 and 2071 to 2100, while for the RCP8.5 scenario, the periods from 2011 to 2040 and 2071 to 2100 would exhibit the most deficit in rainfall. The months of August and September would present surplus compared to the reference period whatever the scenario and the projected period considered. For the RCP4.5 scenario, the period from 2041 to 2070 would present less surplus than the other two projected periods, while for the RCP8.5 scenario, the rate of increase of rainfall amounts relative to the reference period would be increasing until 2100 for the months of August and September. These changes are statistically significant at the 95% confidence level whatever the considered projected period except P1 (July), P3 (July), and P2 (September) for RCP4.5 and P2 (July and October) for RCP8.5 (Table 3). The changes in May are not statistically significant at the 95% confidence level.

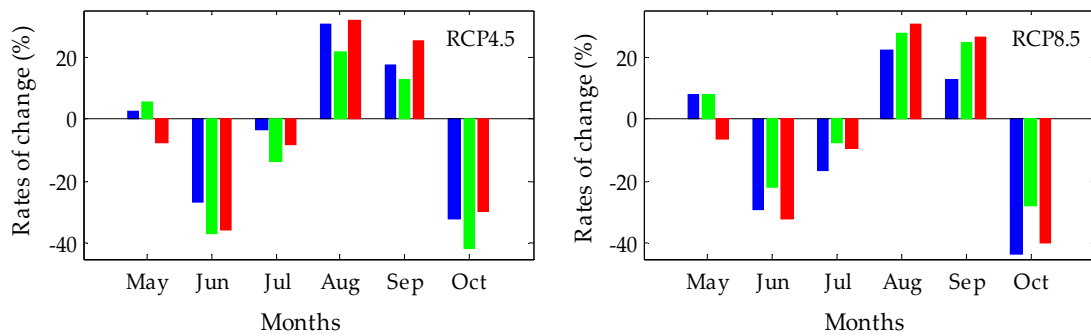


Figure 4. Rates of change of monthly rainfall amounts per projected period and scenario (blue: P1, green: P2 and red: P3).

3.2. Potential Evapotranspiration Change

3.2.1. Annual Change

Table 4 and Figure 5 present the means of annual PET per period and the rates of change over the three different projected periods according to the RCP4.5 and RCP8.5 scenarios. Under both scenarios, there could be an increase of PET until 2100. The increase provided by the RCP8.5 scenario is each time higher than that provided by the RCP4.5 scenario. At the end of the century (2071–2100), the rate of increase provided by the RCP8.5 scenario is twice the rate of the increase provided by the RCP4.5 scenario. The changes are statistically significant at the 95% confidence level (Table 5).

Table 4. Mean of annual PET per period.

Baseline	Projections		
	Periods	RCP4.5	RCP8.5
1587.27 ± 98.21	P1	1626.50 ± 18.04	1652.99 ± 26.57
	P2	1666.14 ± 20.51	1701.98 ± 24.19
	P3	1685.56 ± 25.55	1766.63 ± 31.57

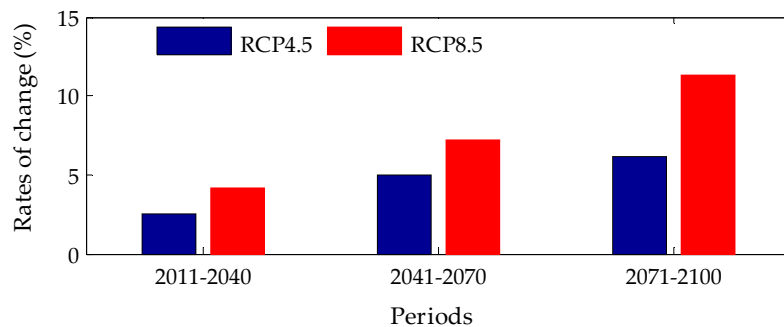


Figure 5. Rates of change of annual PET per projected period and scenario.

Table 5. Results of student's t-test for PET.

Periods	January	February	March	April	May	June	July	August	September	October	November	December	Yearly
RCP4.5													
P1	9.82 *	7.16 *	2.50 *	−2.00 *	−1.85	9.47 *	14.49 *	3.59 *	5.52 *	6.03 *	6.10 *	9.83 *	9.26 *
P2	10.54 *	8.04 *	5.06 *	1.68	0.15	12.10 *	14.59 *	6.31 *	8.27 *	6.83 *	7.08 *	11.18 *	12.10 *
P3	11.61 *	8.49 *	4.93 *	2.98 *	2.66 *	15.34 *	19.01 *	8.45 *	9.68 *	6.96 *	8.50 *	12.22 *	14.02 *
RCP8.5													
P1	10.51 *	8.48 *	3.57 *	−1.00	−1.35	11.02 *	16.17 *	6.04 *	9.19 *	7.55 *	7.20 *	11.55 *	11.20 *
P2	11.78 *	10.18 *	5.73 *	2.30 *	1.69	14.50 *	18.13 *	8.28 *	11.55 *	9.29 *	7.74 *	12.39 *	14.44 *
P3	13.86 *	11.41 *	9.82 *	6.91 *	6.67 *	21.50 *	24.48 *	12.63 *	15.28 *	11.77 *	8.40 *	14.25 *	19.26 *

* States significant difference between the mean of the projected period and the mean the baseline period.

3.2.2. Monthly Change

Figure 6 shows the rates of change in the monthly PET relative to the reference period for the three projected periods under the RCP4.5 and RCP8.5 scenarios. Regardless of the projection period and scenario considered, January, February, March, June, July, August, September, October, November, and December show a statistically significant increase of PET at the 95% confidence level (Table 5) compared to the reference period. These increases are continuous until 2100 for each month. The increases provided by the RCP8.5 scenario are for each month and each projected period, higher than those provided by the RCP4.5 scenario. December, January, June, and July have the highest rates of increase (about from 20% to 30%) for both scenarios and the three projected periods. This can be explained by the fact that these two first months are the warmest months in the basin with no rainfall, and according to the projected rainfall (Table 3) rainfall amounts, would decrease in June and July. February, August, and November indicate increases of PET with rates of about 10% of PET of the reference period regardless of the projected period and scenario considered. This increase is also statistically significant at the 95% confidence level (Table 5). The months of April and May indicate decreases of PET for the RCP4.5 scenario for only P1, while for the other projected period and for RCP8.5, these months indicate increases of PET.

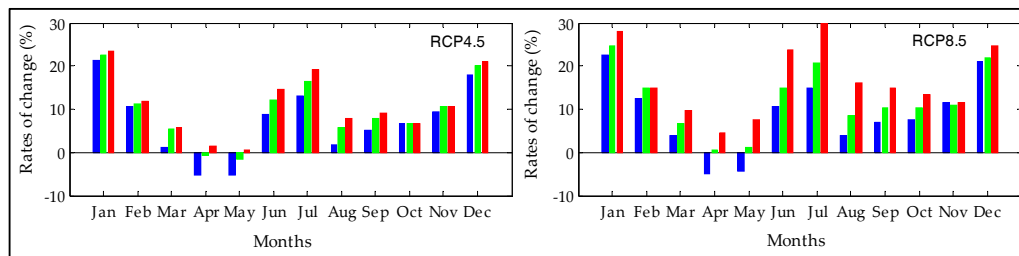


Figure 6. Rates of change of monthly PET per projected period (blue: P1; green: P2 and red: P3).

If for the yearly PET, the RCP4.5 and RCP8.5 scenarios provide a continuous increase until 2100 [9] in the basin, at a monthly scale, we find that some months indicate increases of PET while over months indicate decreases of PET.

3.3. Discharges Simulation

Performances of Hydrological Models

Table 6 and Figure 7 show the performances of hydrological models in calibration and validation for different input data. For the observed meteorological data in the basin, the four hydrological models show a good capacity of reproduction of the daily flows in the Mékrou catchment at the Kompongou outlet. Indeed, the Nash criteria vary from 0.73 to 0.87 in calibration against 0.63 to 0.74 in validation. In calibration, the models AWBM and SimHyd present the best performances with, respectively, 0.87 and 0.85 as values of the Nash criterion, while in validation, it is the ModHyPMA and HBV models which present the best performances with Nash criterion values, respectively, equal to 0.74 and 0.71. The ModHyPMA and HBV models with respect to the small difference between the Nash criterion values obtained in calibration and in validation, are the most robust of the four hydrological models for this catchment. The coefficients of determination vary from 0.86 to 0.88 in calibration against 0.68 to 0.71 in validation for the four models. These results are consistent with those of [35], who tested these models using the same basin but with consecutive calibration and validation periods (1965–1974 and 1975–1984). Referring to [42] on the equifinality problem, which states that the greater the number of parameters to be calibrated for a model is, the easier it is to obtain good performances for this model, one can conclude with the performances of ModHyPMA that this model with only two parameters to be calibrated is better than the three other models which each have a higher number of parameters

to be calibrated (seven for AWBM and SimHyd and nine for HBV). The use of climate model data as input data for hydrological models also yielded very good calibration and validation performances. If, in the calibration with RCMs data, there is a decrease in model performances compared to the values obtained with the observed meteorological data, in validation, the performances of the models with the RCMs data is always higher than those obtained with the observed meteorological data, with the exception of the SimHyd model. The works such as [43] in the north of Tunisia and [44] in Ethiopia also used RCMs data as the input of rainfall-runoff with success.

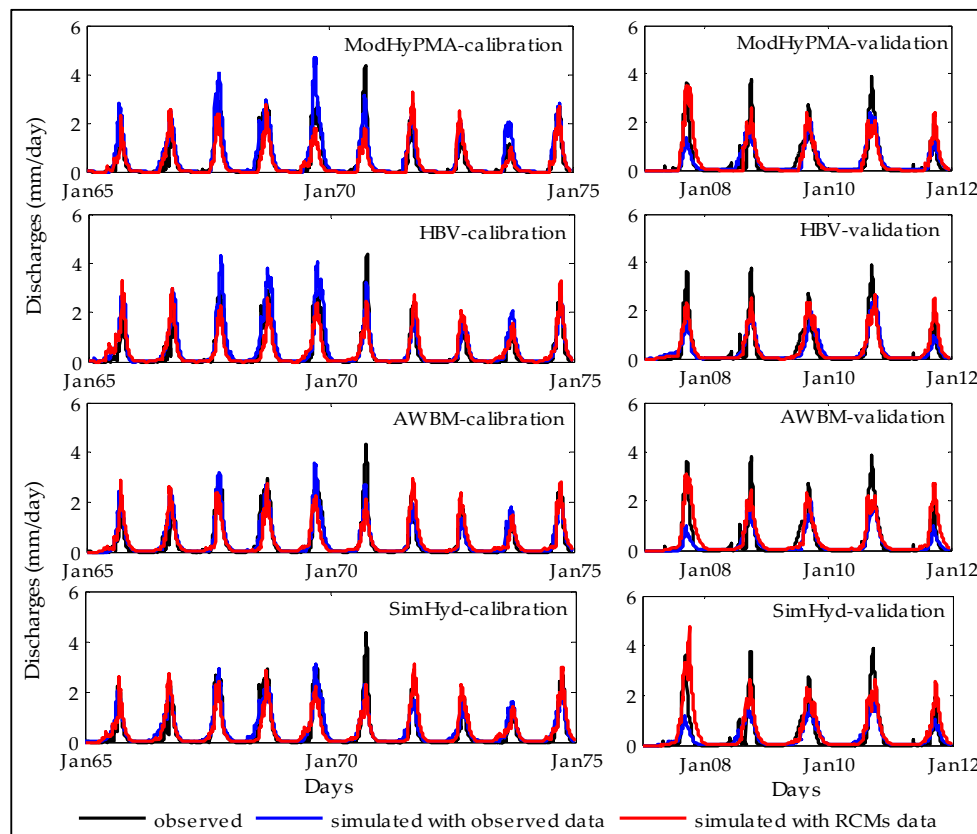


Figure 7. Hydrographs of observed and simulated discharge.

Table 6. Performances of hydrological models in calibration and validation period.

Criterion	Calibration				Validation			
	NSE		R ²		NSE		R ²	
Input data	Observed	RCM	Observed	RCM	Observed	RCM	Observed	RCM
ModHyPMA	0.77	0.70	0.87	0.71	0.74	0.75	0.69	0.71
HBV	0.73	0.71	0.86	0.71	0.71	0.74	0.71	0.75
AWBM	0.87	0.70	0.88	0.7	0.63	0.68	0.68	0.71
SimHyd	0.85	0.71	0.86	0.71	0.61	0.58	0.70	0.66

3.4. Change in Runoff

3.4.1. Annual Change

Figures 8 and 9 show the annual mean of projected discharges. According to the RCP4.5 scenario (Figure 8), the projected flow of the four hydrological models indicates the increases of discharges for different projected periods compared to the baseline period, which is 0.30 mm/day. For the ModHyPMA model, the mean values of the periods P1, P2, and P3 are, respectively, 0.40 mm/day,

0.33 mm/day, and 0.42 mm/day, which represent, respectively, the rates of increase of 33%, 10%, and 40% of discharge compared to the discharge of the baseline period, while for HBV model, the means are 0.46 mm/day, 0.37 mm/day, and 0.44 mm/day, i.e., the increases of 53%, 23%, and 46% compared to the discharge of the baseline period. For the AWBM model, the mean of periods P1 and P3 are equal to 0.44 mm/day (an increase of 46% compared to flows of the reference period), while for the period P2, it is equal to 0.36 mm/day (an increase of 20%). With SimHyd, the mean values of periods P1 and P3 are equal to 0.50 mm/day (an increase 66%), while for the period P2, it is equal to 0.40 mm/day (33% of increase). However, it can be seen that the flows of period P2 are deficient compared to the flows of periods P1 and P3. This flow deficit can be explained by the decrease in rainfall amounts [9] combined with the increase of PET during the P2 period for the RCP4.5 scenario.

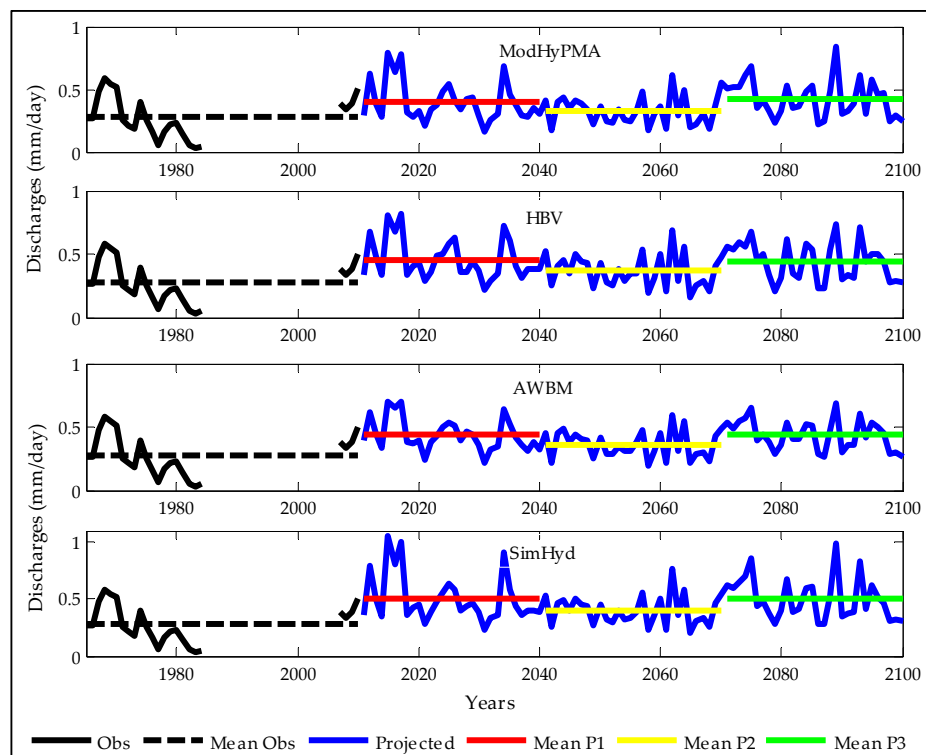


Figure 8. Evolution annual mean of projected discharge according to the RCP4.5 scenario.

According to scenario RCP8.5 (Figure 9), period P2 exhibits the most excess in discharges of the three projected periods. It will be preceded and followed by two deficit periods (P1 and P3). Despite the deficits of periods P1 and P3, the flows of these two periods are in excess compared to the flows of the baseline period. According to the ModHyPMA and HBV predictions, the mean values of periods P1 and P3 are about 0.36 mm/day (20% rate of increase compared to the baseline period) and 0.43 mm/day (43% rate of increase of discharge relative to the baseline period) for period P2. For the AWBM model, the means of the annual discharges of periods P1 and P3 are, respectively, 0.37 mm/day and 0.39 mm/day (respectively, 23% and 30% rates of increase compared to the baseline period) against 0.45 mm/day (50% rate of increase compared to the reference period) for period P2. For the SimHyd model, the means of periods P1 and P3 are, respectively, equal to 0.43 mm/day (43% rate of increase compared to the period Compared to 0.52 mm/day (73% rate of increase compared to the reference period) for period P2. The increases of runoff of the three projected periods relative to the baseline period are statistically significant at the 95% confidence level except for the P1 and P3 projected periods for, respectively, the ModHyPMA and HBV models (Table 7).

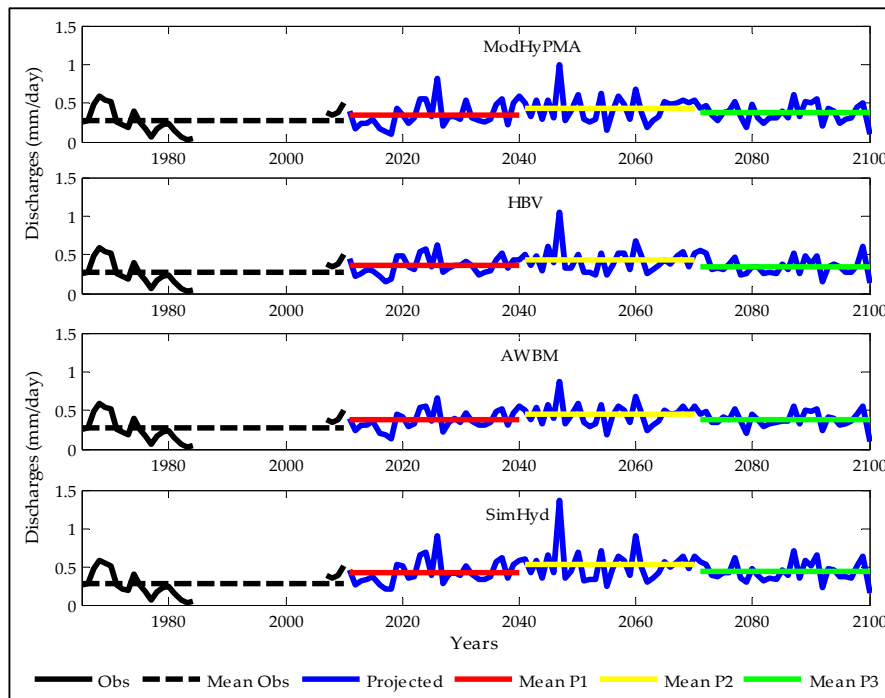


Figure 9. Evolution annual mean of projected discharge according to the RCP8.5 scenario.

3.4.2. Monthly Change

The comparison of the monthly mean hydrographs of projected periods P1, P2, and P3 to the observed hydrograph can allow us to better analyze if the discharge changes are accompanied by a modification of the hydrological regime of the catchment. Figure 10 illustrates the means of monthly hydrographs calculated for the different projected periods (P1, P2, and P3) and for the reference period. The correspondence between the mean hydrographs calculated at the three horizons and the observed hydrograph is quite good. The month in which the peaks of floods occur will stay September regardless of the projected periods. In terms of dynamics, there is no change in hydrological regimes in the basin. The periods of high flow and low flow remain identical to those of the observed period whatever the projected period and the rainfall-runoff model considered. The changes mainly relate to the quantities of flow per month. Thus, the variability of the flows that was observed above would be closely related to the variability of the monthly mean flows during the high water period (the flows from August to October) and not to a change in the hydrological regime of the catchment. There are the most significant increases of the mean monthly discharge from August to November whatever the considered scenario, projected period, and hydrological model (Table 7). These results are consistent with those of [43,44].

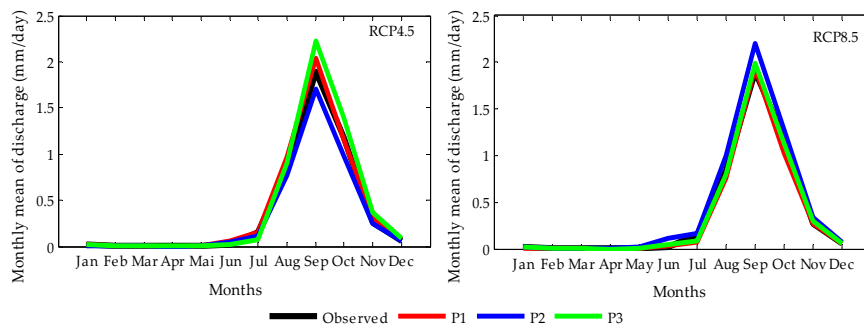


Figure 10. Evolution hydrograph of projected discharge under the RCP4.5 and RCP8.5 scenarios.

Table 7. Results of student's t-test for runoff.

Period	RCP4.5						RCP8.5					
	July	August	September	October	November	Yearly	July	August	September	October	November	Yearly
ModHyPMA												
P1	0.18	3.23 *	2.24 *	2.11 *	3.06 *	2.78 *	−1.51	1.44	1.63	1.21	2.14 *	1.56
P2	−0.54	1.44	0.86	1.01	2.12 *	1.35	0.52	3.16 *	3.01 *	2.83 *	3.63 *	3.46 *
P3	−1.46	2.98 *	3.37 *	3.04 *	3.63 *	3.47 *	−1.09	1.85	2.32 *	2.11 *	2.92 *	2.42 *
AWBM												
P1	0.86	3.42 *	2.64 *	2.56 *	5.71 *	4.09 *	−0.33	1.37	1.64	1.27	4.41 *	2.43 *
P2	0.20	1.36	1.14	1.32	4.53 *	2.31 *	1.00	3.29 *	3.00 *	2.79 *	5.87 *	4.25 *
P3	−0.20	2.60 *	3.27 *	3.21 *	5.94 *	4.26 *	−0.23	1.15	2.12 *	2.05 *	5.15 *	3.00 *
HBV												
P1	2.14 *	3.78 *	3.06 *	3.61 *	3.78 *	4.14 *	1.33	2.07 *	1.26	1.44	2.29 *	2.19 *
P2	0.68	1.67	1.26	2.29 *	2.95 *	2.23 *	2.07 *	3.08 *	2.42 *	3.01 *	3.40 *	3.44 *
P3	0.58	2.59 *	3.27 *	3.85 *	4.02 *	3.86 *	0.80	1.27	1.12	1.80	2.37 *	1.95
SimHyd												
P1	3.09 *	4.73 *	2.97 *	3.42 *	4.88 *	4.43 *	1.91	3.16 *	2.11 *	2.39 *	4.19 *	3.43 *
P2	1.63	2.73 *	1.48	2.37 *	4.31 *	3.08 *	2.97 *	4.39 *	3.41 *	3.83 *	5.13 *	4.67 *
P3	1.63	4.22 *	3.68 *	3.87 *	4.93 *	4.76 *	1.63	2.94 *	2.62 *	3.07 *	4.75 *	3.90 *

* States significant difference between the mean of the projected period and the mean the baseline period.

4. Discussion

The models' performances over the 10-year calibration and the five-year validation periods have been found to be good, implying that the models can reproduce the observed runoff with an acceptable accuracy. However, the ability of the four models to reproduce flows is limited by the poor reproduction of flood flows. In fact, the four hydrological models failed in the reproduction of the exceptional flood of 1970 in the calibration period. The same observation was made for the floods of 2007, 2008, and 2010. The decrease in the performance of the four hydrological models in the validation period can be explained by the difficulty of the models to reproduce the flood flows. But the low flows are well reproduced by the models. Many studies have underlined the inability of hydrological models to estimate flood discharge [45,46]. In this study, the under estimation of high discharge may be due to the determination of the average rainfall in the basin. In fact, the basin with an area of 5670 km² has only two rain gauges and to reach a sufficient number of rain gauges it was resorted to the rain gauges around the catchment and the means of daily rainfall were extracted from the mean of all used rain gauges. Moreover, the frequency of extreme rainfall in the basin can also affect flows. The validation performances with RCMs data is sometimes better than that obtained with the observed data. The use of the in situ data seems to alter the simulation quality. It would be important to test the same hydrological models with gridded data such as the Era-interim reanalysis data [47] and observed precipitation data such as Global Precipitation Climatology Project-GPCP [48] and Tropical Rainfall Mission Measurement (TRMM, 3B42; [49]) to improve the simulation quality. The multi-models approach can also be developed to increase the model performances and reduce the simulation uncertainties.

The study has focused on changes in the future water availability and its temporal availability. The RCP4.5 scenario indicates an increase of annual precipitations in the near-future (P1), while decreases are expected for the middle (P2) and the end century (P3). For the RCP8.5 scenario, the near future is characterized by a decrease of annual precipitations, while the middle and end of the century are characterized by a slight increase. Even if these changes are insignificant, they confirm the changes in past rainfall in the region [9,50]. Many studies have indicated that the RCMs do not converge on future precipitation changes in Western Africa. This is mainly due to model errors and processes representation in RCMs, rather than to differences in driving GCMs [51]. This could also be explained by the great variability of precipitations and a high occurrence of small-scale precipitations in West Africa. Downscaling RCMs with a high spatial resolution of grids (about 5 km) to take into account the low-scale phenomena could therefore improve the performances of RCMs in the region. The monthly projections show significant decreases of precipitation in June, July, and October under both RCP4.5 and RCP8.5 scenarios, while significant increases in August and September are indicated. This means that the rainy season could be concentrated in August and September. So it could therefore have a restriction of the duration of the rainy season and a diminution of the number of wet days as indicated by [9] in the basin and by [10] in Burkina-Faso. If, despite the decreasing of the number of wet days in the basin, the annual averages do not vary significantly, it can be concluded that the frequency of extreme precipitations could increase.

The annual PET projections show a significant increase in the averages of the three projected periods relative to the baseline period for both RCP4.5 and RCP8.5 scenarios. These projections converge with the projections of temperatures in the region. Moreover, as with the temperatures, the increase under the RCP8.5 scenario is higher than that obtained under the RCP4.5 scenario. On a monthly scale, the projections show a significant increase of PET means for all months and all periods except in April and May, which predict a decrease of the mean for the P1 period of the two scenarios. The increase of PET may lead to soil moisture decrease and increase of the water stress of the plants. This can lead to the decline in agricultural production, the destruction of vegetation cover, and the amplification of desertification in this area.

The consequences of climate change on the discharges have also been investigated in this study. The projected discharges indicate a significant increase relative to the baseline period. Despite this

increase, it can be noted that for the RCP4.5 scenario, there is a decrease of discharges in the P2 period compared to the P1 and P3 periods, while for the RCP8.5 scenario, the P2 period flows are lower than the discharges of P1 and P3 periods. The future variation of discharges is strongly related to the precipitation variation for each projected period. The discharges will therefore depend heavily on rainfall in the basin. The increase of flows during the P2 period can be explained by the large increase of rainfall over the catchment during this period for the RCP8.5 scenario [9]. Similar results were obtained by [52,53] in the Indus basin in Pakistan. Ref. [54] also found a high variability in future flows due to the variability of the various components of the hydrological cycle in the same catchment. As with rainfall, the significant runoff increases were obtained mostly from August to November. Otherwise, the convergence of the projections of all the hydrological models implies that these models are robust in the context of climate change. The combination of these four hydrological models in a multi-model can also improve the performance of the projections and especially reduce the uncertainties on the forecasts.

5. Conclusions

This paper first allowed us to estimate, using data from an ensemble of three climate models, the change in rainfall and PET in the Mékrou catchment at the Kompngou outlet in the short, medium, and long-term. If there is a continuing increasing trend to 2100 for PET for both RCP4.5 and RCP8.5 scenarios, rainfall variability will be observed depending on the projected periods and the climate change scenario considered. The method used to compute an ensemble climate model output is the Simple Average Method. It will be important to use other methods such as the Weighted Average Method that take into account the performance of each model in ensemble approach computing. An increase in the number of climate models is also required to reduce the uncertainties of models. Despite the quality of the EQM method in bias correction, the use of several bias correction methods could be helpful for assessing their impact on hydrological simulations in this catchment. Future studies could focus on these aspects.

From four hydrological rainfall-runoff models, the daily flows in the basin were simulated with the observed data and those from the climate models. Based on the results obtained, it appears that the hydrological models used have shown a good capacity for the simulation of flows at the outlet of Kompongou with RCMs data as the input. This good capacity can be improved by developing the multi-models approach in the catchment.

Acknowledgments: There is no funding for this study.

Author Contributions: Eric Adéchina Alamou, Ezéchiél Obada, and Abel Afouda designed the study, developed the methodology, and wrote the manuscript. Eric Adéchina Alamou and Ezéchiél Obada performed the field work, collected the data, and conducted the computer analysis, while Abel Afouda supervised this part of the work.

Conflicts of Interest: The authors declare no conflict of interest.

References

1. Intergovernmental Panel on Climate Change (IPCC). Summary for Policymakers. In *Climate Change 2014: Impacts, Adaptation, and Vulnerability*; Contribution of Working Group II to the Fifth Assessment Report of the Intergovernmental Panel on Climate Change; Cambridge University Press: Cambridge, UK; New York, NY, USA, 2014.
2. Barrios, S.; Ouattara, B.; Strobl, E. The impact of climatic change on agricultural production: Is it different for Africa? *Food Policy* **2008**, *33*, 287–298. [[CrossRef](#)]
3. Giorgi, F.; Coppola, E.; Raffaele, F. A consistent picture of the hydroclimatic response to global warming from multiple indices: Models and observations. *J. Geophys. Res. Atmos.* **2014**, *119*. [[CrossRef](#)]

4. Zwiers, F.W.; Alexander, L.V.; Hegerl, G.C.; Knutson, T.R.; Kossin, J.; Naveau, P.; Nicholls, N.; Schär, C.; Seneviratne, S.I.; Zhang, X. Challenges in estimating and understanding recent changes in the frequency and intensity of extreme climate and weather events. In *Climate Science for Serving Society: Research, Modeling and Prediction Priorities*; Springer: Berlin, Germany, 2013.
5. Intergovernmental Panel on Climate Change (IPCC). *Climate Change 2007—Synthesis Report*; Cambridge University Press: Cambridge, UK, 2007.
6. Sylla, M.B.; Nikiema, P.M.; Gibba, P.; Kebe, I.; Klutse, N.A.B. Climate change over West Africa: Recent trends and future projections. In *Adaptation to Climate Change and Variability in Rural West Africa*; Springer: Basel, Switzerland, 2016.
7. Sylla, M.B.; Elguindi, N.; Giorgi, F.; Wisser, D. Projected robust shift of climate zones over West Africa in response to anthropogenic climate change for the late 21st century. *Clim. Chang.* **2016**, *134*, 241–253. [[CrossRef](#)]
8. Tall, M.; Sylla, M.B.; Diallo, I.; Pal, J.S.; Faye, A.; Mbaye, M.L.; Gaye, A.T. Projected impact of climate change in the hydroclimatology of Senegal with a focus over the Lake of Guiers for the twenty-first century. *Theor. Appl. Climatol.* **2017**, *129*, 655–665. [[CrossRef](#)]
9. Obada, E.; Alamou, E.A.; Zandagba, E.J.; Chabi, A.; Afouda, A. Change in future rainfall characteristics in the Mekrou Catchment (Benin), from an ensemble of 3 RCMs (MPI-REMO, DMI-HIRHAM5 and SMHI-RCA4). *Hydrology* **2017**, *4*, 14. [[CrossRef](#)]
10. Ibrahim, B.; Karambiri, H.; Polcher, J.; Yacouba, H.; Ribstein, P. Changes in rainfall regime over Burkina Faso under the climate change conditions simulated by 5 regional climate models. *Clim. Dyn.* **2014**, *42*, 1363–1381. [[CrossRef](#)]
11. Cook, K.H.; Vizy, E.K. Impact of climate change on mid-twenty-first century growing seasons in Africa. *Clim. Dyn.* **2012**, *39*, 2937–2955. [[CrossRef](#)]
12. Elguindi, N.; Grundstein, A.; Bernardes, S.; Turuncoglu, U.; Feddema, J. Assessment of CMIP5 global model simulations and climate change projections for the 21st Century using a modified Thornthwaite climate classification. *Clim. Chang.* **2014**, *122*, 523–538. [[CrossRef](#)]
13. Akinsanola, A.A.; Ogunjobi, K.O.; Gbode, I.E.; Ajayi, V.O. Assessing the capabilities of three regional climate models over CORDEX Africa in simulating West African summer monsoon precipitation. *Adv. Meteorol.* **2015**, *2015*, 935431. [[CrossRef](#)]
14. Yira, Y.; Diekkrüger, B.; Steup, G.; Bossa, A.Y. Impact of climate change on hydrological conditions in a tropical West African catchment using an ensemble of climate simulations. *Hydrol. Earth Syst. Sci.* **2017**, *21*, 2143–2161. [[CrossRef](#)]
15. Sarr, A.B.; Camara, M.; Diba, I. Spatial distribution of cordex regional climate models biases over West Africa. *Int. J. Geosci.* **2015**, *6*, 1018–1031. [[CrossRef](#)]
16. GLEauBe. *Etude Portant État Des Lieux et Gestion de L'information sur les Ressources en eau Dans le Bassin de la Mékrou*; Rapport Technique: Cotonou, Benin, 2012; p. 104.
17. Benoit, M. *Statut et Usages du sol en Périphérie du Parc National du "w" du Niger. Tome 1 Contribution à L'étude du Milieu Naturel et des Ressources Végétales du Canton de Tamou et du Parc du "W"*; ORSTOM: Bondy, France, 1998.
18. Christensen, O.B.; Drews, M.; Christensen, J.H. The HIRHAM Regional Climate Model Version 5. Available online: http://orbit.dtu.dk/fedora/objects/orbit:118724/datastreams/file_8c69af6e-acfb-4d1aaa53-73188c001d36/content (accessed on 15 February 2017).
19. Jacob, D.; Bärring, L.; Christensen, O.B.; Christensen, J.H.; Hagemann, S.; Hirschi, M.; Kjellström, E.; Lenderink, G.; Rockel, B.; Schär, C.; et al. An inter-comparison of regional climate models for Europe: Design of the experiments and model performance. *Clim. Chang.* **2007**, *81*, 31–52. [[CrossRef](#)]
20. Samuelsson, P.; Jones, C.G.; Willén, U.; Ullerstig, A.; Gollvik, S.; Hansson, U.; Kjellström, E.; Nikulin, G.; Wyser, K. The Rossby Centre regional climate model RCA3: Model description and performance. *Tellus A* **2011**, *63*, 4–23. [[CrossRef](#)]
21. Obada, E.; Alamou, A.E.; Zandagba, E.J.; Biao, I.E.; Chabi, A.; Afouda, A. Comparative study of seven bias correction methods applied to three Regional Climate Models in Mekrou Catchment (Benin, West Africa). *IJCET* **2016**, *6*, 1831–1840.
22. Déqué, M. Frequency of precipitation and temperature extremes over France in an anthropogenic scenario: Model results and statistical correction according to observed values. *Glob. Planet. Chang.* **2007**, *57*, 16–26. [[CrossRef](#)]

23. Arnaud, M.; Emery, X. *Estimation and Spatial Interpolation: Deterministic Methods and Geostatistics Methods*; Hermès: Paris, France, 2000; p. 221.
24. Cressie, N. *Statistics for Spatial Data*; Wiley: New York, NY, USA, 1992; pp. 613–617.
25. Matheron, G. Regionalized variables theory and its applications. In *Note Book of Mathematical Morphology Centre*; Fasc. 5 EMP: Paris, France, 1971; p. 212.
26. Allen, R.; Periera, L.; Raes, D.; Smith, M. *FAO Irrigation and Drainage: Crop Evapotranspiration (Guidelines for Computing Crop Water Requirements)*; Paper No. 56; FAO: Rome, Italy, 1996.
27. Afouda, A.; Alamou, A.E. Modèle hydrologique basé sur le Principe de Moindre Action (ModHyPMA). *Ann. Sci. Agron.* **2010**, *13*, 23–45. [[CrossRef](#)]
28. Bergström, S.; Forsman, A. Development of a conceptual deterministic rainfall runoff model. *Nord. Hydrol.* **1973**, *14*, 147–170.
29. Boughton, W.C. An Australian water balance model for semiarid watersheds. *J. Soil Water Conserv.* **1995**, *50*, 454–457.
30. Boughton, W. The Australian water balance model. *Environ. Model. Softw.* **2004**, *19*, 943–956. [[CrossRef](#)]
31. Chiew, F.H.S.; Siriwardena, L. Estimation of SIMHYD parameter values for application in ungauged catchments. In *Proceedings of the MOD-SIM 2005 International Congress on Modelling and Simulation. Modelling and Simulation Society of Australia and New Zealand, Melbourne, Australia, 12–15 December 2005*; pp. 2883–2889.
32. Alamou, A.E. Application du Principe de Moindre Action à la Modélisation Pluie-Débit. Ph.D. Thesis, Université d'Abomey Calavi, Abomey Calavi, Benin, 2011; p. 231.
33. Gaba, C.; Alamou, E.; Afouda, A.; Diekkrüger, B. Improvement and comparative assessment of a hydrological modelling approach on 20 catchments of various sizes under different climate conditions. *Hydrol. Sci. J.* **2017**, *62*, 1499–1516. [[CrossRef](#)]
34. Gaba, O.U.C.; Biao, I.E.; Alamou, A.E.; Afouda, A. An ensemble approach modelling to assess water resources in the Mékrou Basin, Benin. *IJCET* **2015**, *3*, 22–32.
35. Obada, E.; Alamou, A.E.; Afouda, A. Evaluation des Performances de Neuf (09) Modèles Hydrologiques Pluie-débit Globaux sur le Bassin de la Mékrou à L'exutoire de Kompongou (Bénin). *Eur. J. Sci. Res.* **2016**, *140*, 411–424.
36. Seibert, J. *HBV Light*, version 2; User's Manual; Department of Physical Geography and Quaternary Geology, Stockholm University: Stockholm, Sweden, 2005; p. 32.
37. Podger, G.M. *Rainfall-Runoff Library User Guide*; Cooperative Research Centre for Catchment Hydrology: Canberra, Australia, 2003; p. 100. Available online: www.toolkit.net.au/rrl (accessed on 20 September 2015).
38. Seibert, J. Multi-criteria calibration of a conceptual runoff model using a genetic algorithm. *Hydrol. Earth Syst. Sci.* **2000**, *4*, 215–224. [[CrossRef](#)]
39. Zhang, X.; Water, D.; Ellis, R. Evaluation of Simhyd, Sacramento and GR4J rainfall runoff models in two contrasting Great Barrier Reef catchments. In *Proceedings of the 20th International Congress on Modelling and Simulation, Adelaide, Australia, 1–6 December 2013*.
40. McCloskey, G.L.; Ellis, R.J.; Waters, D.K.; Stewart, J. PEST hydrology calibration process for source catchments—applied to the Great Barrier Reef, Queensland. In *Proceedings of the 19th International Congress on Modelling and Simulation, Perth, Australia, 12–16 December 2011*; pp. 2359–2366.
41. Moriasi, D.N.; Arnold, J.G.; Van Liew, M.W.; Bingner, R.L.; Harmel, R.D.; Veith, T.L. Model evaluation; guidelines for systematic quantification of accuracy in watershed simulations. *Am. Soc. Agric. Biol. Eng.* **2007**, *50*, 885–900.
42. Beven, K. A manifesto for the equifinality thesis. *J. Hydrol.* **2006**, *320*, 18–36. [[CrossRef](#)]
43. Foughali, A.; Trambly, Y.; Bargaoui, Z.; Carreau, J.; Ruelland, D. Hydrological modeling in Northern Tunisia with regional climate model outputs: Performance evaluation and bias-correction in present climate conditions. *Climate* **2015**, *3*, 459–473. [[CrossRef](#)]
44. Abebe, E.; Kebede, A. Assessment of climate change impacts on the water resources of megech river catchment, Abbay Basin, Ethiopia. *Open J. Mod. Hydrol.* **2017**, *7*, 141–152. [[CrossRef](#)]
45. Tian, Y.; Booij, M.J.; Xu, Y.P. Uncertainty in high and low flows due to model structure and parameter errors. *Stoch. Environ. Res. Risk Assess.* **2014**, *28*, 319–332. [[CrossRef](#)]
46. Akhtar, M.; Ahmad, N.; Booij, M.J. Use of regional climate model simulations as input for hydrological models for the Hindukush–Karakorum–Himalaya region. *Hydrol. Earth Syst. Sci.* **2009**, *13*, 1075–1089. [[CrossRef](#)]

47. Adler, R.F.; Huffman, G.J.; Charney, J.G.; Chang, A.; Ferraro, R.; Xie, P.P.; Janowiak, J.; Rudolf, B.; Schneider, U.; Curtis, S.; et al. The version-2 global precipitation climatology project (GPCP) monthly precipitation analysis (1979–Present). *J. Hydrometeorol.* **2003**, *4*, 1147–1167. [[CrossRef](#)]
48. Huffman, G.J.; Bolvin, D.T.; Nelkin, E.J.; Wolff, D.B.; Adler, R.F.; Gu, G.; Hong, Y.; Bowman, K.P.; Stocker, E.F. The TRMM Multisatellite Precipitation Analysis (TMPA): Quasi-global, multiyear, combined-sensor precipitation estimates at fine scales. *J. Hydrometeorol.* **2007**, *8*, 38–55. [[CrossRef](#)]
49. Rudolf, B.; Becker, A.; Schneider, U.; Meyer-Christoffer, A.; Ziese, M. The New “GPCC Full Data Reanalysis Version 5” Providing High-Quality Gridded Monthly Precipitation Data for the Global Land-Surface Is Public Available since December 2010. In *GPCC Status Report*; GPCC: Offenbach, Germany, 2010; p. 7.
50. Servat, E.; Paturol, J.E.; Lubès-Niel, H.; Kouamé, B.; Masson, J.M.; Travaglio, M.; Marieu, B. De différents aspects de la variabilité de la pluviométrie en Afrique de l’ouest et centrale non sahélienne. *J. Water Sci.* **1999**, *12*, 363–387. [[CrossRef](#)]
51. Paeth, H.; Hall, N.M.; Gaertner, M.A.; Alonso, M.D.; Moumouni, S.; Polcher, J.; Ruti, P.M.; Fink, A.H.; Gosset, M.; Lebel, T. Progress in regional downscaling of West African precipitation. *Atmos. Sci. Lett.* **2011**, *12*, 75–82. [[CrossRef](#)]
52. Ali, S.; Li, D.; Congbin, F.; Khan, F. Twenty first century climatic and hydrological changes over Upper Indus Basin of Himalayan region of Pakistan. *Environ. Res. Lett.* **2015**, *10*, 014007. [[CrossRef](#)]
53. Khan, F.; Pilz, J.; Amjad, M.; Wiberg, D.A. Climate variability and its impacts on water resources in the Upper Indus Basin under IPCC climate change scenarios. *Int. J. Glob. Warm.* **2015**, *8*, 46–69. [[CrossRef](#)]
54. Hasson, S. Future water availability from Hindukush-Karakoram-Himalaya upper indus basin under conflicting climate change scenarios. *Climate* **2016**, *4*, 40. [[CrossRef](#)]



© 2017 by the authors. Licensee MDPI, Basel, Switzerland. This article is an open access article distributed under the terms and conditions of the Creative Commons Attribution (CC BY) license (<http://creativecommons.org/licenses/by/4.0/>).